AD-A253 267

OFFICE OF NAVAL RESEARCH

Contract N00014-82K-0612

R&T CODE: 4133032

TECHNICAL REPORT NO. 76

Template-Synthesis of Infrared-Transparent Metal Microcylinders: Comparison of Optical Properties with the Predictions of Effective Medium Theory

by

C. A. Foss, Jr., M. J. Tierney and C. R. Martin

Prepared for publication

in

Journal of Physical Chemistry

DTIC
ELECTE
JUL 30 1992
S A D

Department of Chemistry
Colorado State University
Ft. Collins, CO 80523

July 20, 1992

Reproduction in whole or part is permitted for any purpose of the United States Government

This document has been approved for public release and sale; its distribution is unlimited

92 7 28 060

92-20410

REPORT DOCUMENTATION PAGE

OMB No 0704-0188

Public reporting burden for this collection of information is estimated to average 1 hour per response, including the time for reviewing instructions, searching existing data sources, gathering and maintaining the data needed, and completing and reviewing the collection of information. Send comments regarding this burden estimate or any other aspect of this collection of information, including suggestions for reducing this burden to Washington Headquarters Services, Directorate for information Operations and Reports, 1215 Jefferson Davis Highway, Suite 1204, Arlington, VA 22202-4302, and to the Office of Management and Budget, Paperwork Reduction Project (0704-0188), Washington, DC 20503

1. AGENCY USE ONLY (Leave blank)	2. REPORT DATE	3. REPORT TYPE AND DATES COVERED
	7-2 - 1992	Interim

4. TITLE AND SUBTITLE
Template-Synthesis of Infrared-Transparent Metal Microcylinders: Comparison of Optical Properties with the Predictions of Effective Medium Theory.

5. FUNDING NUMBERS
Contract
N00014-82K-0612

6. AUTHOR(S)
C. A. Foss, Jr., M. J. Tierney and C. R. Martin

7. PERFORMING ORGANIZATION NAME(S) AND ADDRESS(ES)
Dr. Charles R. Martin
Department of Chemistry
Colorado State University
Fort Collins, CO 80523

8. PERFORMING ORGANIZATION REPORT NUMBER
ONR TECHNICAL REPORT # 76

9. SPONSORING / MONITORING AGENCY NAME(S) AND ADDRESS(ES)
Office of Naval Research
800 North Quincy Street
Arlington, VA 22217

10. SPONSORING / MONITORING AGENCY REPORT NUMBER

11. SUPPLEMENTARY NOTES

12a. DISTRIBUTION / AVAILABILITY STATEMENT
Reproduction in whole or part is permitted for any purpose of the United States Government. This document has been approved for public release and sale; its distribution is unlimited.

12b. DISTRIBUTION CODE

13. ABSTRACT *(Maximum 200 words)*

See attached.

14. SUBJECT TERMS
Transparent metals, nanomaterials, effective medium theory

15. NUMBER OF PAGES

16. PRICE CODE

17. SECURITY CLASSIFICATION OF REPORT	18. SECURITY CLASSIFICATION OF THIS PAGE	19. SECURITY CLASSIFICATION OF ABSTRACT	20. LIMITATION OF ABSTRACT
		UNCLASSIFIED	

ABSTRACT

Metal-insulator composites of varying metal volume fraction have been prepared by electrochemical deposition of gold into porous aluminum oxide membranes. The cylindrical pore array structure of the host oxide serves as a template for the formation of Au particles ca. 0.26 μm in diameter with lengths ranging from 0.3 μm to 3 μm depending on deposition time. The composites display a significant transparency in the infrared spectrum between 2000 and 4000 cm^{-1}. The Au volume fraction and effective medium theory screening parameter κ were estimated from scanning electron microscopic analyses of cylinder dimensions and orientations in the composite membranes. Comparison of experimental spectra with those calculated using Maxwell-Garnett or Bruggeman theories indicates that neither approach is entirely satisfactory. The spectra are consistent, however, with retarded polarization effects due to non-negligible Au particle separation distances in the composites.

Template-Synthesis of Infrared-Transparent Metal Microcylinders: Comparison of Optical Properties with the Predictions of Effective Medium Theory.

Colby A. Foss, Jr., Michael J. Tierney†, and Charles R. Martin*

Department of Chemistry, Colorado State University

Fort Collins, Colorado 80523

Accesion For
NTIS CRA&I ☑
DTIC TAB ☐
Unannounced ☐
Justification
By
Distribution /
Availability Codes
Dist | Avail and / or Special
A-1

†Present address:
Tekṅekron Sensor Development Corp.
1080 Marsh Road, Menlo Park CA 94025

*Author to whom correspondence should be addressed.

DTIC QUALITY INSPECTED 2

ABSTRACT

Metal-insulator composites of varying metal volume fraction have been prepared by electrochemical deposition of gold into porous aluminum oxide membranes. The cylindrical pore array structure of the host oxide serves as a template for the formation of Au particles ca. 0.26 μm in diameter with lengths ranging from 0.3 μm to 3 μm depending on deposition time. The composites display a significant transparency in the infrared spectrum between 2000 and 4000 cm^{-1}. The Au volume fraction and effective medium theory screening parameter κ were estimated from scanning electron microscopic analyses of cylinder dimensions and orientations in the composite membranes. Comparison of experimental spectra with those calculated using Maxwell-Garnett or Bruggeman theories indicates that neither approach is entirely satisfactory. The spectra are consistent, however, with retarded polarization effects due to non-negligible Au particle separation distances in the composites.

I. Introduction

Recently, Aspnes, et al. described the microstructural limits for metal-insulator composites that are both electronically conductive and optically transparent [1]. They predicted that the optimal metal particle geometry for transparency in unpolarized light consists of long narrow cylinders arranged with their principal axes parallel to the direction of light incidence (see Figure 1). We have recently shown that microporous alumina membranes can be used as templates to prepare arrays of metal microcylinders which have this optimal microgeometry [2]. The cylindrical pores of anodically grown Al_2O_3 membranes [3] serve as templates for the electrochemical deposition of parallel arrays of metal microcylinders. The resulting Au/Al_2O_3 composites were shown to display significant transparency in the infrared region of the spectrum [2].

The optical and dielectric properties of composite materials are often discussed in the context of effective medium theory (EMT) [4]. Effective medium theory attempts to predict the optical properties of a composite material from: 1) the optical constants of the components in their pure form; 2) the volume fraction of each component; and 3) the shape and orientation of the component particles in the composite. The Au/Al_2O_3 composites investigated here are ideal model systems for evaluating theoretical models because the host oxide structure insures a parallel alignment of the metal particles. Also, the aspect ratios of these particles can be controlled by varying the amount of metal deposited.

In this paper we compare experimental transmittance spectra of Au/Al_2O_3 composites containing different amounts of of Au with those calculated using EMT. We focus primarily on the Maxwell-Garnett (MG) treatment because it is appropriate for metal particles that are isolated from each other by a layer of the insulating component (in this case the pore walls of the host oxide). However, we also discuss the self-consistent Bruggeman (BR) approach which treats the composite as a random mixture of both metallic and insulating particles [6].

Both the MG and BR models are based on the Clausius-Mossotti equation [4], which is formally valid only for static electric fields [7]. In an optical experiment, where we are dealing with electromagnetic radiation (i.e., photon fields), there is the complication of photon scattering [4,8,10]. However, if the particle dimensions and their mutual separation distances are small relative to the wavelength of light, scattering effects can be considered negligible. This situation is often referred to as the "quasi-static" or infinite wavelength limit of effective medium theory [4,8].

In the recent literature the practical limits of quasi-static models are often discussed with regard to particle size. An often cited criterion for the applicability of quasi-static models is that the ratio of the particle diameter d to the wavelength of light employed (d/λ) should be less than 0.1 [4,10]. In this report we demonstrate that while our composites fulfil this criterion over most of the spectral range considered, they are not completely amenable to quasi-static treatments. The infrared transmittance spectra are, however, amenable to a modified MG approach that takes into account particle separation distances that are not negligible relative to the wavelength of the incident light [11].

II. Summary of Effective Medium Theory Concepts in the Quasi-Static Limit and Consequences for Composite Transparency.

A. The Maxwell-Garnett and Bruggeman Treatments

The general relationship between the composite's effective dielectric function ε and the dielectric functions of the metal compo-

nent ε_m and the insulating component ε_o is based on an extension of the Clausius-Mossotti equation [4,7]

$$\frac{\varepsilon - \varepsilon_h}{\varepsilon + K\varepsilon_h} = f_m \frac{\varepsilon_m - \varepsilon_h}{\varepsilon_m + K\varepsilon_h} + f_o \frac{\varepsilon_o - \varepsilon_h}{\varepsilon_o + K\varepsilon_h} \qquad (1)$$

where f_m and f_o are the volume fractions of the metal and insulator, respectively. The screening parameter K depends on the shapes of the component particles and the orientation of these particles with respect to the electric field. This factor will be discussed further below.

The host function ε_h describes the dielectric constant experienced by the component particles at the microscopic level. The Maxwell-Garnett (MG) model assumes that at all metal volume fractions, the metal particles are surrounded by a layer of insulating material [4,8]. Hence the host function ε_h is assumed equal to ε_o. Equation 1 then reduces to

$$\frac{\varepsilon - \varepsilon_o}{\varepsilon + K\varepsilon_o} = f_m \frac{\varepsilon_m - \varepsilon_o}{\varepsilon_m + K\varepsilon_o} \qquad (2a)$$

or, in its more convenient form

$$\varepsilon = \varepsilon_o \frac{f_m K(\varepsilon_m - \varepsilon_o) + \varepsilon_m + K\varepsilon_o}{\varepsilon_m + K\varepsilon_o - f_m(\varepsilon_m - \varepsilon_o)} \qquad (2b)$$

In contrast, the Bruggeman treatment (BR) assumes that the composite contains a random mixture of metal and insulator particles. The host function cannot be identified with ε_o because at some critical volume fraction of metal, the metal particles must begin to touch each other. In this case then, ε_h is assumed equal to ε. Equation 1 thus becomes [4]

$$f_m \frac{\varepsilon_m - \varepsilon}{\varepsilon_m + K\varepsilon} + f_o \frac{\varepsilon_o - \varepsilon}{\varepsilon_o + K\varepsilon} = 0 \qquad (3a)$$

or, alternatively,

$$K\varepsilon^2 + \{\varepsilon_m(f_m K - f_o) + \varepsilon_o(f_o K - f_m)\}\varepsilon - \varepsilon_m\varepsilon_o = 0 \qquad (3b)$$

The practical difference between these two treatments is that for a given metal fraction and K, the MG model predicts a higher transmittance than the BR approach.

B. The Screening Parameter and Particle Shape.

The particle screening parameter k is related to the Lorentz depolarization factor q through [4]

$$K = \frac{(1 - q)}{q} \qquad (4)$$

The depolarization factor depends on the geometry of the particle and its orientation with respect to the electric field. In the present work, we assume that the gold microcylinders can be treated as ellipsoids of revolution as shown in Figure 2. If the axis of revolution **a** is parallel to the incidence vector (and hence perpendicular to the electric field E), a simple relation based on the magnitudes of **a** and the semi-minor axis **b** provides a very good approximation for q [12]:

$$q \approx \frac{1/b}{1/a + 2/b} \qquad (5)$$

Figure 3 shows how q and κ vary as a function of the particle aspect ratio **a/b**. If the particle is flat and disc-like (**a/b** is small), q is close to zero and κ is very large. In the case of a sphere, **a** and **b** are equal and equations 4 and 5 lead to the expected results [4] for q = 1/3 and $\kappa = 2$. As **a** becomes very large relative to **b**, q approaches 1/2 and κ approaches unity; these are the limits for long narrow cylinders discussed by Aspnes, et al. [1].

C. The Ideal Limits for Composite Transparency

As was mentioned in section IIA, the MG model predicts a higher transparency than the BR model for given values of f_m and κ. Hence, if optical transparency is the goal [1,2] it is important to maintain electrical isolation of the metal particles in the composite. A second important issue concerns the magnitude of ε_m. As $|\varepsilon_m|$

approaches infinity, equation 2 reduces to

$$\varepsilon = \varepsilon_o \frac{(f_m K + 1)}{(1 - f_m)} \qquad (6)$$

From equation 6, it can be seen that the composite dielectric constant will most resemble that of the insulating component when $|\varepsilon_m|$ is very large and when K is small. In the present study we focus on a range of infrared wavelengths where the Al_2O_3 absorption coefficient k_o is essentially zero (note that $\varepsilon o = (n_o + ik_o)^2$). Furthermore, $|\varepsilon_m|$ for Au is large in the infrared spectrum. Also, since the Au inclusions are cylindrical, K can be minimized. Therefore, the systems investigated here should approach the ideal case for optical transparency as defined by equation 6.

III. Experimental

A. Sample Preparation

Porous aluminum oxide membranes (Anopore^R, pore diameters nominally 0.20μm, Alltech Associates) were first sputtered [2] with silver to provide a conductive backing; as indicated in Figure 4A, this Ag film is too thin to block the pores of the membrane. The membrane was then placed sputtered side down on a glass plate that was partially covered with an aluminum foil electrical contact (we found that wetting the glass plate prior to application of the Ag/Anopore^R membrane such that there was an even sheet of distilled water between the glass and the oxide, led to more even Ag deposition). Ag was deposited galvanostatically at current densities between 0.8 and 1.0 mA cm^{-2} (Figure 4B). The plating solution was as per reference 14. In all cases the amount of Ag deposited was 6.5 Coulombs. The purpose of this Ag plating step was to make

"foundations" for the subsequent deposition of Au particles. These foundations are necessary because Anopore^R membranes have interconnected pores near the surface [13]. The Ag foundations insure that the subsequently-deposited Au particles are not deposited in this interconnected region.

After the silver deposition step, the cell was rinsed thoroughly with distilled water. Gold was then deposited potentiostatically at -0.90 Volts versus an Ag/AgCl reference (Figure 4C). The Au(I) plating solution was obtained from a commercial source (Technics Orotemp). We prepared six sets of samples in which 0.5, 1.0, 2.0, 3.0, 4.0 and 5.0 Coulombs of Au were deposited over the 3.46 cm^2 membrane area. After thorough rinsing, the cell was dismantled and the composite transferred to a watch glass containing 3 to 5 M nitric acid. This step removes the silver foundation, leaving behind the gold microcylinders (Figure 4D).

The cell used in this study was similar to that described in reference 2, except that the deposition area was smaller (in the present case 3.46 cm^2) and N_2 purging was used, instead of a magnetic stir bar, for mixing. An EG&G Princeton Applied Research 173 potentiostat equipped with a PARC 176 coulometer was used for both Ag and Au deposition procedures.

B. Electron Microscopic Analyses

Characterization of the composite membranes and gold particles was done using a Philips 505 scanning electron microscope (SEM). Two types of analyses were done. In the first , the Au/Anopore^R composites were fractured and SEM micrographs were obtained of the fractured edges of the membranes. The second SEM analysis involved investigations of isolated Au particles. The Au particles were isolated by dissolving the Anopore^R in 0.2M NaOH. The solutions were then filtered over 0.1 μm-pore diameter polycarbonate filters (Poretics, Inc.). In order to reduce errors in the electron microscopic determination of microcylinder length and diameter measurements, the polycarbonbate filters were sputtered with gold before the filtration step. The Au-coated filters containing

the free gold cylinders were then attached to SEM sample stubs with silver epoxy.

C. *Spectroscopic Measurements*

Infrared transmittance spectra were obtained using a Mattson Galaxy 4021 FTIR.

IV. Results

A. *Microstructure*

Figure 5A shows an SEM micrograph of a cross-section of an Au/Anopore^R membrane composite. The Au cylinders are positioned deep within the membrane, ca. 10 μm from the nearest membrane face. Furthermore, because of dispersion in the lengths of the Ag foundations, the Au cylinders are scattered somewhat relative to the membrane face. The SEM shown in Figure 5A indicates that the microcylinder array can be modelled as shown in Figure 5B, where d_2 is the average thickness of the composite layer containing the Au microcylinders, and d_1 and d_3 are the average distances from the composite region to the membrane faces. This three-layer model (metal-free region of thickness d_1, metal containing region of thickness d_2, and metal free region of thickness d_3) is the basis for comparison with the predictions of EMT. As will be discussed below, the parameter d_2 defines the composite optical path length and is also an important factor in the estimate of the metal volume fraction f_m.

The measurement of cylinder lengths required the dissolution of the Anopore^R host and subsequent collection of the Au particles on a filter membrane (edge views such as in Figure 5 involve fracturing of the membrane and may lead to Au cylinder breakage). Figures 6A through 6C show SEM micrographs of free Au particles on

polycarbonate filter membranes. The amounts of Au deposited were 0.5, 3 and 5 coulombs for Figures 6A, 6B and 6C, respectively. Figure 7 shows the relationship between the amount of Au deposited and the average cylinder length as determined from SEM micrographs. As would be expected, a linear relationship is observed.

B. Estimates of the Screening Parameter κ.

Figures 6 and 7 demonstrate that microparticle dimensions can be controlled by varying the amount of metal deposited. While the cylinder diameters are constant at 0.26(±0.05) μm, the lengths are easily varied between ca. 0.3 and 3 μm. From the length and diameter of the Au microcylinders, the depolarization factor q and screening parameter κ can be calculated using equations 4 and 5 in Section II. Table I summarizes the results of these calculations for the six different samples. As the amount of Au deposited increases, the particles become more needle-like and κ approaches unity. At the lower end, the particles are more sphere-like and κ is close to 2.

C. Estimates of the Metal Volume Fraction f_m *and Composite Optical Path Length* d_2.

By taking into account the total deposit area A, the atomic weight and density of Au, and the number of coulombs delivered, we can relate the cylinder length l_{cyl} to the host membrane porosity P through

$$l_{cyl} = \frac{(\text{No. Coulombs Au(I)})(\text{atomic weight Au})}{(96{,}485)\, A\, \rho_{Au}\, P} \qquad (7a)$$

or,

$$l_{cyl}\ (\mu m) = 0.313\ \frac{(\text{No. Coulombs Au(I)})}{P} \qquad (7b)$$

From this relation and the slope of the plot of l_{cyl} versus the number of coulombs (Figure 7) the host membrane porosity was found to be 0.57 (± 0.03).

The inherent porosity of the host oxide is important because it represents the upper limit for the metal volume fraction f_m. If the Au cylinders were positioned at a uniform distance from the membrane face, the composite thickness d_2 shown in Figure 5B would simply be l_{cyl}, and f_m would be given by P. In fact, because the cylinder placement is not uniform (see Figure 5), the composite thickness d_2 is greater than l_{cyl} and the metal volume fraction f_m is less than P. We assume that f_m is thus given by the relation

$$f_m = l_{cyl}\ P/d_2 \qquad (8)$$

The composite optical path d_2 is assumed to be a function of the cylinder length and the standard deviation δd_1 in cylinder position relative to the nearest face. We calculate d_2 via

$$d_2 = l_{cyl} + 2\delta d_1 \qquad (9)$$

From SEM micrographs of the composite film edges (e.g., Figure 5A) and the measurement of d_1 in 107 cylinders, δd_1 is estimated to be ca. 1.35 μm. Table I summarizes the calculated values of f_m and d_2 according to equations 8 and 9, respectively.

D. Experimental Spectra

Figure 8 shows the infrared transmittance spectra of a blank Anopore^R membrane and spectral averages of Au/Anopore^R composites where 0.5, 1.0, 2.0, 3.0, 4.0 and 5.0 coulombs of Au(I)

were deposited inot the pores.. These quantities of deposited Au correspond to Au microcylinders with lengths of ca. 0.33, 0.66, 1.23, 1.58, 2.28 and 2.99 μm, respectively (see Table I). The averages are based on the spectra of three samples, except in the case of the 4.0 coulomb set, where two samples were measured. The standard deviations in %T at 2000 cm^{-1} range from 1.7% in the 3.0 coulomb set to 4.2% in the 0.5 coulomb samples. These low standard deviations indicate that the composite preparation procedure leads to reproducible optical properties.

In all cases, the composite samples show a transmittance maximum at ≈ 2000 cm^{-1}. At lower energies, the host Al_2O_3 absorbs strongly. As we reported in our previous paper, there is a gradual loss in transmittance as the incident energy increases from 2000 wavenumbers [2]. A broad shallow band at 3500 cm^{-1} is attributed to $Al(OH)_n$ species [15].

E. Calculation of Spectra

It was mentioned in the introduction that the quasi-static limit is met when the diameter of the particles are about one-tenth that of the incident wavelength [4]. In this study, we are dealing with cylindrical geometries where the cylinder *length* in some cases exceeds the wavelength. Examination of the experimental spectra (see Figure 8) indicates that the reduction in transmittance between 2000 cm^{-1} and 4000 cm^{-1} is in fact only weakly dependent on cylinder length. We thus assume for the remainder of the discussion that quasi-static EMT limits depend on cylinder diameter; cylinder length operates only to affect K, f_m, and composite path length d_2.

SEM analysis of the composite membranes and free Au cylinders indicates that the Au particles are isolated from each other by the pore walls of the host oxide. Hence, the MG formulation of EMT should be more appropriate. However, for comparison we calculate spectra on the basis of both the MG and BR models. In both cases the calculation involves resolving the given EMT expression

(equation 2b or 3b) into its real and imaginary components ε' and ε'', respectively. The refractive index n_2 and absorption coefficient k_2 of the composite layer (of thickness d_2) can then be obtained from the well-known relations [16]

$$\varepsilon' = n_2^2 - k_2^2 \qquad (14a)$$

$$\varepsilon'' = 2n_2k_2 \qquad (14b)$$

The optical constants n_m and k_m for Au were taken from the compilations of Lynch and Hunter [17]. For the n_o and k_o values for anodic aluminum oxide, we rely on the data of Harris [18]. The Au volume fraction and screening parameter K are taken from Table I.

The absorption loss for each component of the three layer model shown in Figure 5B is given by [19]

$$T_{abs,i} = e^{-4\pi k_i d_i/\lambda} \qquad (15)$$

where k_i and d_i are the absorption coefficient and optical path length, respectively, for a given layer. Reflective losses at each interface in the three layer model were calculated using [19]

$$T_{R,i} = 1 - \frac{(n_{i+1} - n_i)^2 + (k_{i+1} - k_i)^2}{(n_{i+1} + n_i)^2 + (k_{i+1} + k_i)^2} \qquad (16)$$

The total transmittance in the three layer system is thus given by

$$T_{tot} = \prod_{i=0}^{3} T_{R,i} \cdot \prod_{i=1}^{3} T_{abs,i} \qquad (17)$$

where i=0 and i=3 pertain to the two interfaces between the host oxide and air.

F. Comparisons with Maxwell-Garnett and Bruggeman Theories

Figure 9 shows infrared spectra calculated according to the procedure outlined in the previous section using the MG model (equation 2). The parameters f_m, K and d_2 are taken from the average values given in Table I. The plots are in qualitative agreement with the experimentally observed trends; the total transmittance decreases with increasing incident energy and cylinder length. However, in all cases the calculated transmittance is higher than seen in experiment. Attempts to fit the experimental spectra by varying f_m, K and d_2 were unsuccessful: First, matching the transmittances at 2000 cm^{-1} required f_m values that exceed the inherent porosity of the host oxide. Second, even if a certain combination of parameters led to a fit at 2000 cm^{-1}, the same set resulted in an overestimate of %T at 4000 cm^{-1}.

Simulated spectra based on the BR model and f_m, K and d_2 values in Table I are shown in Figure 10. In this case, the transmittance drops dramatically at higher energies, particularly with higher values of f_m. The experimental spectra corresponding to the composites with the lowest volume fractions of Au (see curves 2 and 3 in Figure 8) seemed somewhat amenable to a fit procedure based on the BR model; however, in all other cases parameters leading to a fit at 2000 cm^{-1} led to a severe underestimation of transmittance at 4000 cm^{-1}.

Finally, it should be noted that we utilized existing optical data for Al_2O_3 [18] ; we made no attempt to model the broad surface hydroxide band at ca. 3500 cm^{-1}.

G. The Maxwell-Garnett Model Modified for Retarded Polarization.

It may be reasonable to conclude that the failure of the Maxwell-Garnett and Bruggeman treatments to model the experimental spectra stems from gold particles that are too large relative to the wavelength of the incident light for scattering effects to be ignored. We therefore calculated the transmittance of films containing gold spheres 0.26 μm in diameter using Mie scattering theory [12,20]. Since the Mie calculations actually overestimated the transmittance at all wavelengths when compared to the Au/Anopore^R films containing short sphere-like particles, it would seem that the gold particle diameter is not the principal cause of transmittance losses in our composites.

We mentioned in the introduction that, in addition to particle size, the spacing of the metal, particles in the insulating matrix is an important factor in determining the optical properties of the composite. Consider a metal particle surrounded by an insulating medium and other metal particles. When the composite ensemble is exposed to light, the electric field experienced by a metal particle is the sum of the incident field and the induced fields arising in the other metal particles. If the metal particles and their separation distances are small, the induced and incident fields are virtually in phase and the total field experienced by the ensemble can be considered uniform [10,11]. This situation justifies the volume-average approach to the composite polarizability which is central to the quasi-static effective medium treatment.

On the other hand, if metal particle separations are not small relative to the wavelength, there is a phase lag between the incident and induced fields experienced by a given particle. This condition is referred to as retarded polarization [11]. Granqvist and Hunderi

have proposed the following modification to account for particle separation effects for an ensemble of spherical particles [11]:

$$\varepsilon = \varepsilon_o \frac{\{\varepsilon_o + (1/3)(\varepsilon_m - \varepsilon_o) + (1 - (1/3)e^{i\delta})f_m(\varepsilon_m - \varepsilon_o)\}}{\{\varepsilon_o + (1/3)(\varepsilon_m - \varepsilon_o) - (1/3)e^{i\delta}f_m(\varepsilon_m - \varepsilon_o)\}} \quad (18)$$

where $\delta = 2\pi a_s(n_o + ik_o)/\lambda$ and a_s is the average particle separation distance. As one would expect, as δ approaches zero equation 18 reduces to the simple MG expression given by equation 2b for q = 1/3 and κ = 2. While Granqvist and Hunderi discuss retarded polarization only for spherical microstructures, we assume for the present case that equation 18 can be generalized by replacing "1/3" with a q-value appropriate to other geometries such as the cylindrical particles in our composites.

In Figure 11 we compare experimental spectra to those calculated using equation 18 with the separation factor a_s as a fit parameter. The fit procedure involved a simple least-squares analysis of experimental transmittances at 2000 and 4000 cm-1. The parameters f_m, d_2 and κ were allowed to vary in a manner internally consistent with equations 4, 5, 8 and 9 and a host porosity of 0.57. In all cases the fit results are quite satisfactory. Furthermore, except in the first two samples, the fits are accomplished with values of f_m, κ and d_2 within the limits of error suggested in Table I. In the first two samples which contain the lowest amounts of deposited Au, the fit results for f_m seem somewhat high, but do not exceed the inherent porosity of the aluminum oxide host. A summary of fit parameters is given in Table II.

The values of a_s obtained from the least-squares fit are consistent with SEM micrographs, which indicate a pore wall thickness of ca. 0.15 μm. However, since the particles are scattered somewhat relative to the membrane face, their mutual separation is expected to be greater than the pore wall thickness.

V. Conclusions

We have presented a method for the preparation of metal-insulator composites which allows for the control of the metal volume fraction and the screening parameter κ. The porous Anopore^R host material insures the electrical isolation of the metal particles, thus maximizing composite transparency even at moderate metal volume fractions. The Au/Anopore^R composites discussed here display a significant transparency in the infrared spectrum despite cylinder lengths as high as 3 μm and metal volume fractions of ca. 20%.

The infrared spectra are not, however, completely amenable to quasi-static effective medium treatments. We have shown that this can be explained on the basis of separation distances that are not negligible relative to the wavelength of the incident radiation. Hence, it is clear that in addition to particle size, particle separation is an important consideration in the preparation of transparent metal microstructure materials.

In this study we relied on commercial sources for the aluminum oxide host membranes, and were thus limited to pore diameters that are relatively large. Our discussion has therefore been limited to the infrared region of the spectrum. However, because pore size and porosity can be varied through anodizing conditions [3,21], anodic aluminas are ideal templates for the control of small metal particle size and shape.

Acknowledgements

We gratefully acknowledge the financial support of the Office of Naval Research, Washington, D.C.

References

1. Aspnes, D.E.; Heller, A; Porter, J.D. *J. Appl. Phys.*, 1986, 60, 3028.

2. Tierney, M.J.; Martin, C.R. *J. Phys. Chem.*, 1989, 93, 2878.

3. Thompson, G.E.; Wood, G.C., in Scully, J.C. (Ed.), "*Treatise on Material Science and Technology*", Academic Press, New York, 1983, Vol. 23.

4. Aspnes, D.E. *Thin Solid Films*, 1982, 89, 249.

5. Maxwell-Garnett, J.C. *Philos. Trans. R. Soc. London*, 1904, 203, 385.

6. Bruggeman, D.A.G. *Ann. Phys. (Leipzig)*, 1935, 24, 636.

7. Atkins, P.W. "*Physical Chemistry*", Second Edition, W.H. Freeman, San Francisco, 1982, pp 772-3

8. Stroud, D.; Pan, F.P. *Phys. Rev. B*, 1978, 17, 1602.

9. Lamb, W.;Wood, D.M.;Ashcroft, N.W. *Phys. Rev. B.*, 1980, 21, 2248.

10. Smith, G.B. *Appl. Phys. Lett.*, 1979, 35, 668.

11. Granqvist, C.G.; Hunderi, O. *Phys. Rev. B*, 1977, 16, 1353.

12. van de Hulst, H.C. "*Light Scattering by Small Particles*", Dover, New York, 1981.

13. Furneaux, R.C.;Rigby, W.R.; Davidson, A.P. U.S. Patent No. 4,687,551. August 18, 1987.

14. Shumilova, N.A.; Zutaeva, G.V. in Bard, A.J. (Ed.), "*Encyclopedia of Electrochemistry of the Elements*", Marcel Dekker, New York, 1978, Vol. 8, p. 109.

15. Wefers, K.; Misra, C. "*Oxides and Hydroxides of Aluminum*", Alcoa Technical Paper No. 17 (Revised), Alcoa Laboratories, 1987.

16. Bard, A.J.; Faulkner, L.R. "*Electrochemical Methods*", Wiley, New York, 1980, p. 586.

17. Lynch, D.W.; Hunter, W.R. in Palik, E. (Ed.), "*Handbook of Optical Constants of Solids*", Academic Press, New York, 1985. p. 294.

18. Harris, L. *J. Opt. Soc. Amer.*, 1955, 45, 27.

19. Abeles, F. in van Heel, A.C.S. (Ed.), "*Advanced Optical Techniques*", North Holland Publ. Co., Amsterdam, 1967, pp. 143-188.

20. We employed the first four terms in the Mie expansion discussed by van de Hulst. See pp 269-271 in reference 12 for details.

21. Foss, C.A., Jr.; Hornyak, G.L.; Stockert, J.A.; Martin, C.R. *J. Phys. Chem.* (accepted for publication)

Table I

Composite Microstructural Parameters

Coulombs Au	$l_{cyl}(\mu m)^a$	$d_2(\mu m)^b$	$f_m{}^c$	q^d	K^e
0.5	0.33 ±0.10	3.03 ±0.10	0.06 ±0.03	0.36 ±0.12	1.8 ±0.7
1.0	0.66 ±0.12	3.36 ±0.20	0.11 ±0.03	0.42 ±0.10	1.39 ±0.19
2.0	1.23 ±0.22	3.93 ±0.22	0.17 ±0.04	0.45 ±0.10	1.21 ±0.16
3.0	1.58 ±0.25	4.28 ±0.25	0.20 ±0.05	0.46 ±0.11	1.16 ±0.35
4.0	2.28 ±0.35	4.98 ±0.35	0.25 ±0.06	0.47 ±0.11	1.11 ±0.35
5.0	2.99 ±0.53	5.69 ±0.53	0.28 ±0.07	0.48 ±0.11	1.09 ±0.34

[a]From SEM micrographs. [b]Calculated from equation 9 where $\delta d_1 \approx$ 1.35 μm (see text). [c]Calculated from equation 8 where P = 0.57. [d,e]Calculated from l_{cyl} and equations 4 and 5 where the cylinder diameter is 0.26 (± 0.05) μm in all cases.

Table II

Figure 11 Fit Parameters for Granqvist-Hunderi Modification of Maxwell-Garnett Model.

Curve	$l_{cyl}(\mu m)$	f_m	$d_2(\mu m)$	q	$a_s(\mu m)$
1	0.40	0.27	0.86	0.38	0.25
2	0.66	0.20	1.92	0.42	0.25
3	1.23	0.19	3.70	0.45	0.20
4	1.50	0.21	4.12	0.46	0.20
5	2.00	0.23	5.04	0.47	0.22
6	2.60	0.26	5.68	0.48	0.18

Figure Captions:

Figure 1. Optimum microstructure for metal-insulator composite transparency in circularly polarized light (from reference 1).

Figure 2. Orientation of an ellipsoid of revolution with respect to electric field and axes relevant to the estimation of the depolarization factor q via equation 5.

Figure 3. Variation of depolarization factor q (3A) and K (3B) with ellipsoid aspect ratio, a/b, based on equations 5 and 4, respectively.

Figure 4. Fabrication procedure for Au/Anopore^R composite. A) Ag is sputtered on one side of host Al_2O_3 membrane. B) Membrane is placed sputtered side down onto a glass plate and Ag foundation is deposited electrochemically. C) Au is electrochemically deposited onto Ag foundations. D) Ag is removed with nitric acid.

Figure 5. A) Scanning electron micrograph (SEM) of Au/Anopore^R composite cross-section. Sample shown was fabricated by deposition of 5 C of Au(I) onto a 3.46 cm^2 area of alumina membrane. B) Three-layer model for Au/Anopore^R composite systems employed in spectral simulations.

Figure 6. SEM micrographs of Au particles after host Anopore^R has been dissolved. Au content in coulombs Au(I) deposited onto 3.46 cm^2 area: A) 0.5 C; B) 3.0 C; C) 5.0 C.

Figure 7. Measured Au cylinder lengths as a function of the number of coulombs delivered in Au electrodeposition step. Standard deviations based on number of measurements shown in parentheses.

Figure 8. Infrared transmittance spectra of blank Anopore^R membrane (curve 1) and Au/AnoporeR composites. Composite spectra according to number of coulombs Au(I) deposited on 3.46 cm^2 area: Curve 2, 0.5 C; Curve 3, 1.0 C; Curve 4, 2.0 C; Curve 5, 3.0 C; Curve 6, 4.0 C; Curve 7, 5.0 C.

Figure 9. Simulated transmittance spectra based on Maxwell-Garnett model. Input parameters taken from averages given in Table I: 0.5 C (◇), 1.0 C (◆), 2.0 C (○), 3.0 C (●), 4.0 C (△), 5.0 C (▲).

Figure 10. Simulated transmittance spectra based on Bruggeman model. Input parameters taken from averages given in Table I: 0.5 C (□), 1.0 C (■), 2.0 C (▽), 3.0 C (▼), 4.0 C (○), 5.0 C (●).

Figure 11. Comparison between experimental infrared spectra and calculations based on Granqvist-Hunderi modification of Maxwell-Garnett Theory. Experimental curves (solid) as defined in Figure 8. Calculated curves based on parameters summarized in Table II.

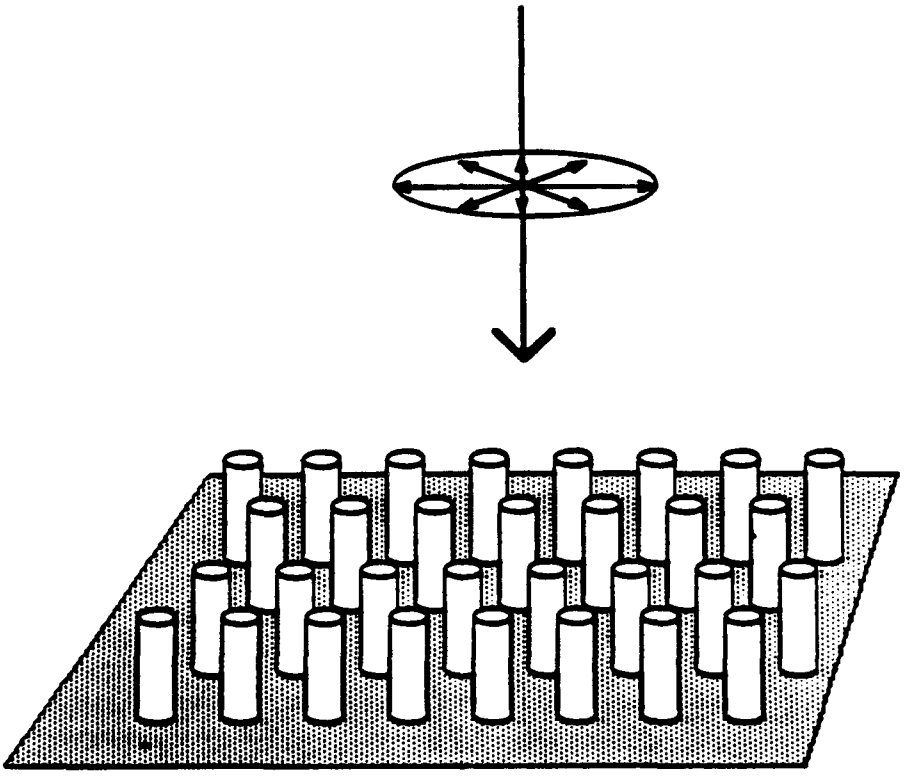

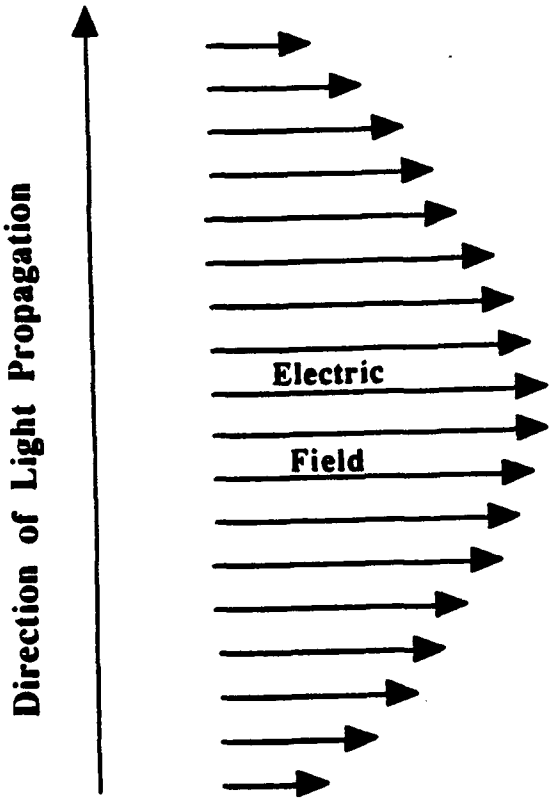

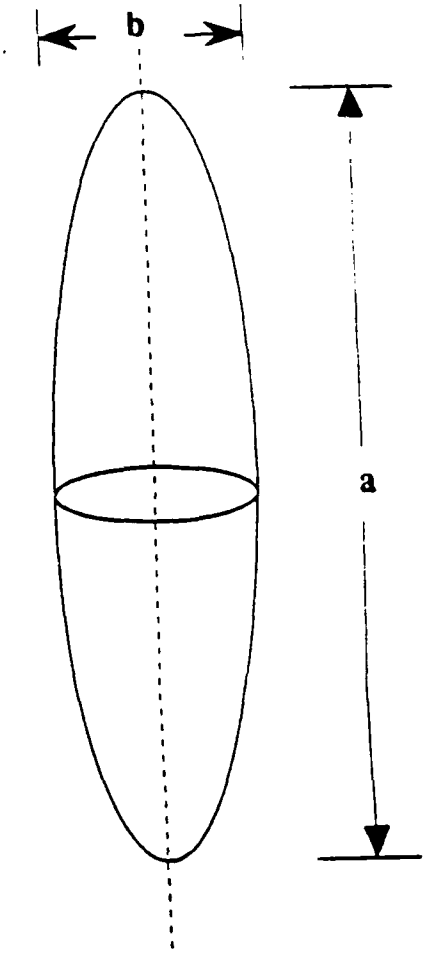

Au Particle

A

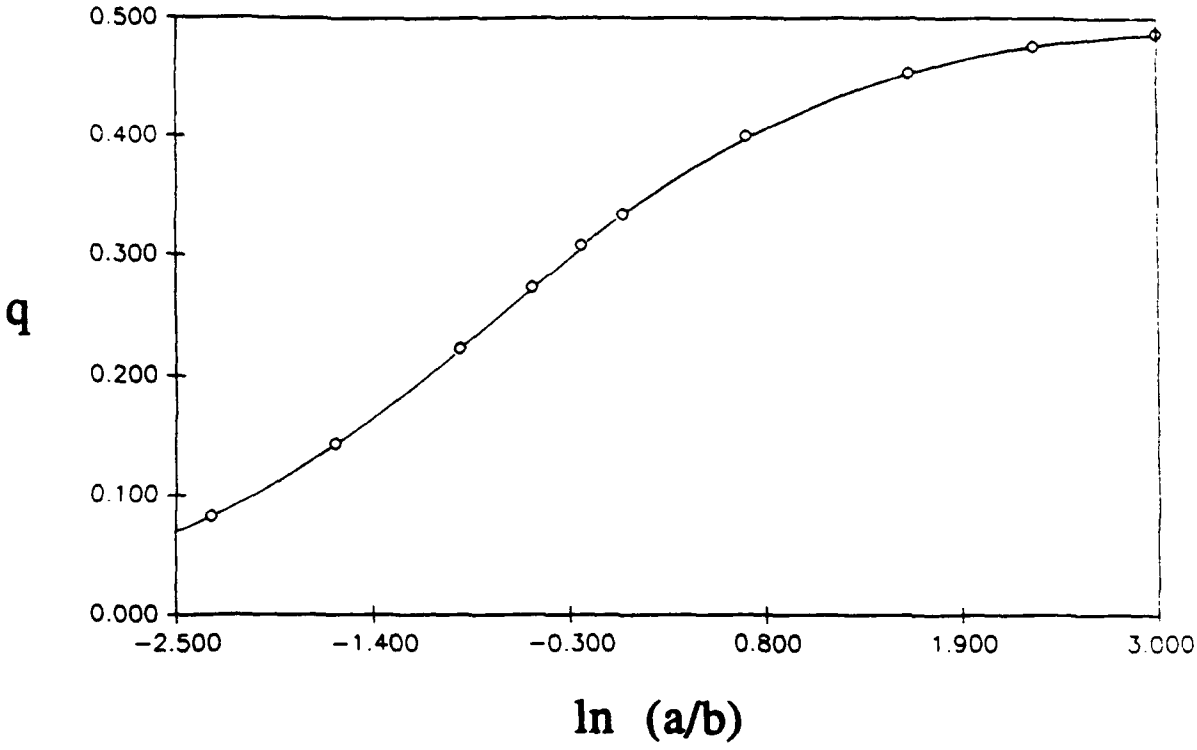
0.500
0.400
0.300
0.200
0.100
0.000
q
−2.500
−1.400
−0.300
0.800
1.900
3.000
ln (a/b)

B

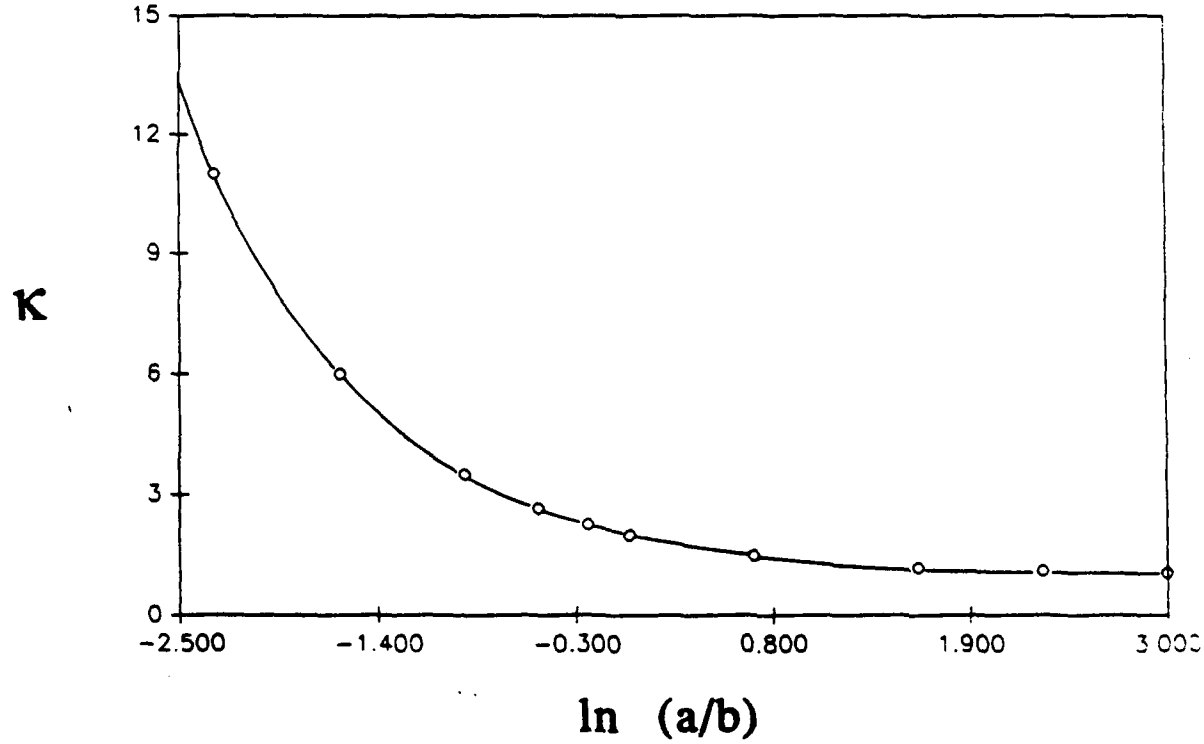
15
12
9
6
3
0
κ
−2.500
−1.400
−0.300
0.800
1.900
3.000
ln (a/b)

F2

A. Ag Sputter

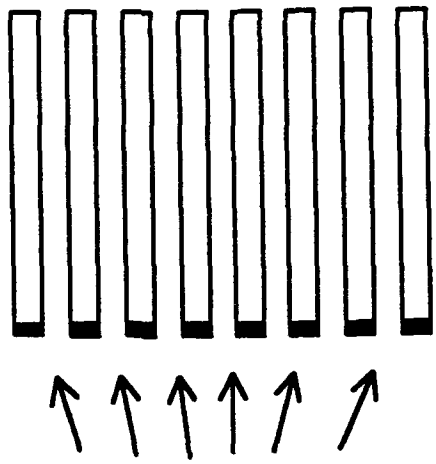

B. Electrodeposit Ag

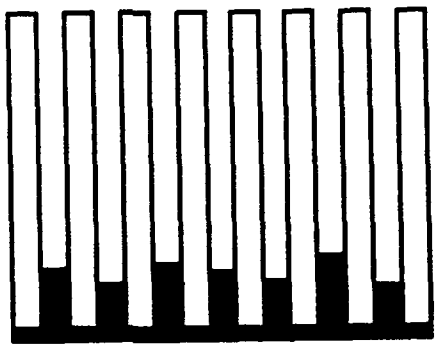

C. Electrodeposit Au

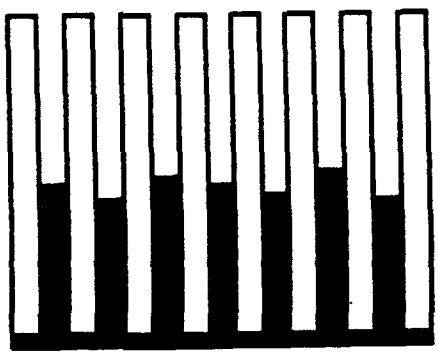

D. Nitric Acid Wash

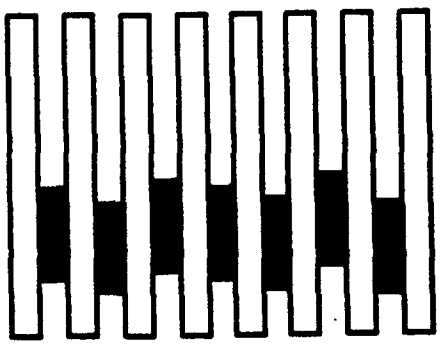

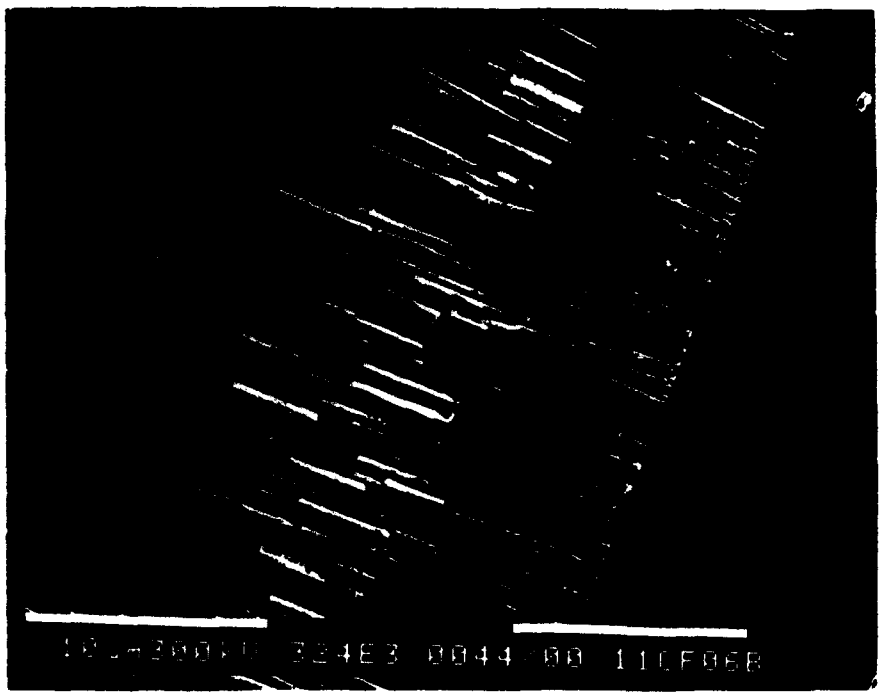

A

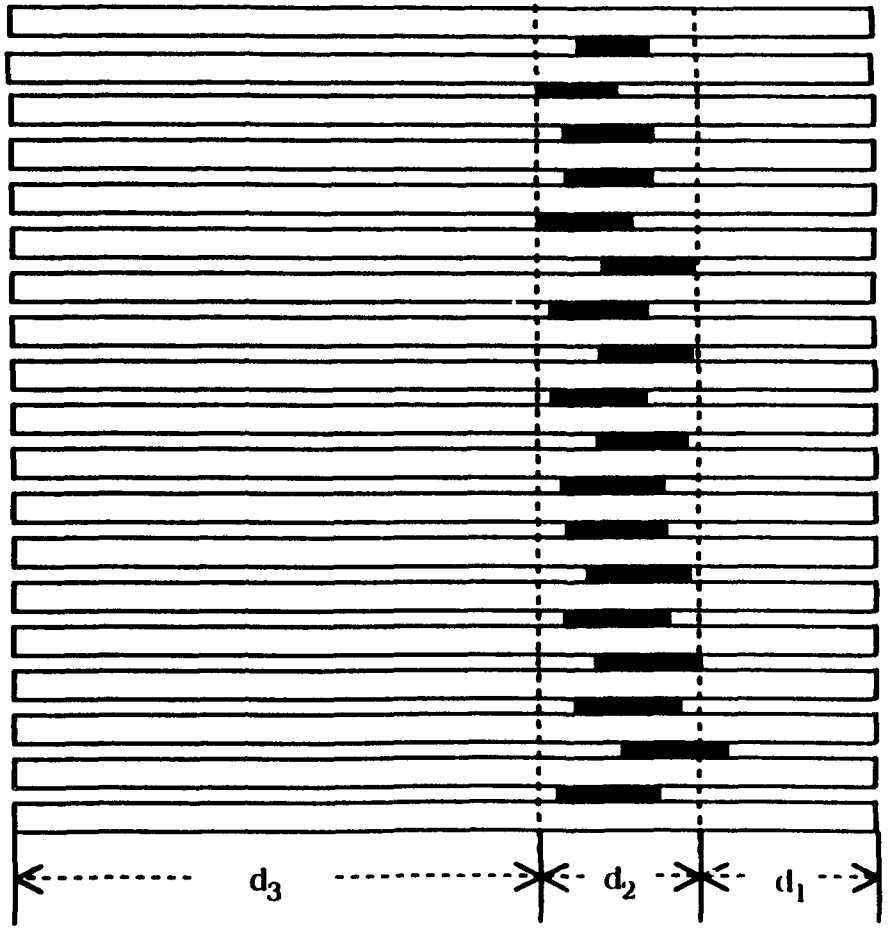

B

A

B

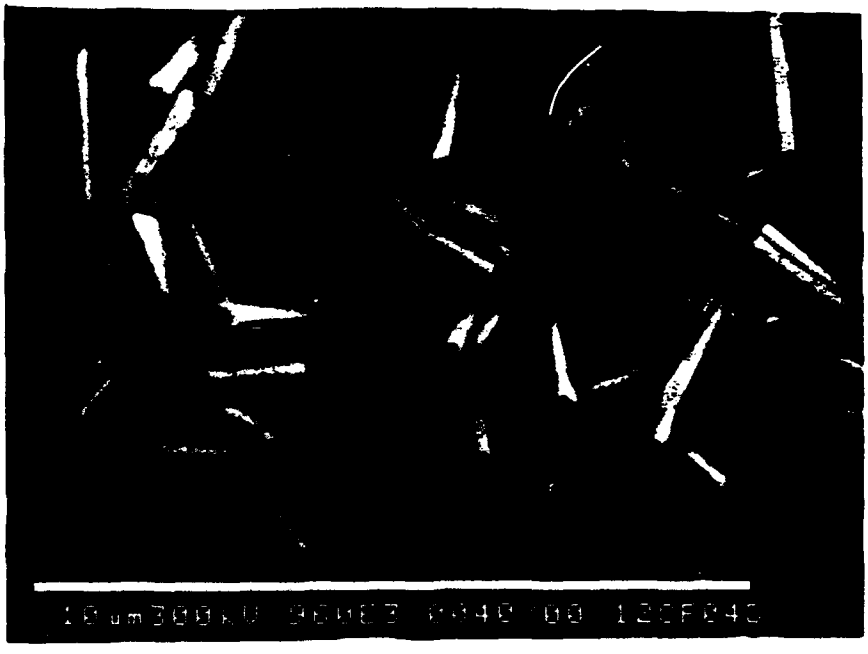

C

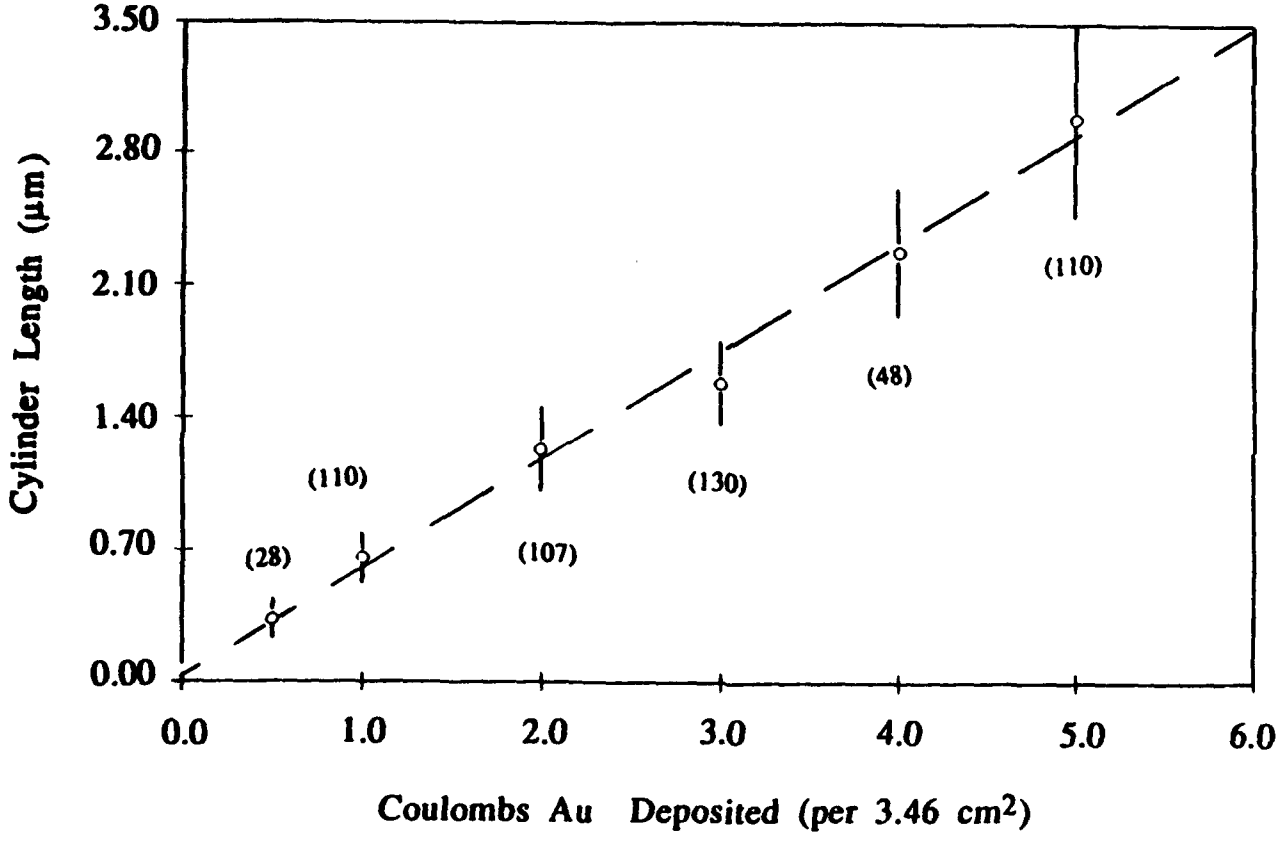
3.50
2.80
2.10
1.40
0.70
0.00
Cylinder Length (μm)
(28)
(110)
(107)
(130)
(48)
(110)
0.0
1.0
2.0
3.0
4.0
5.0
6.0
Coulombs Au Deposited (per 3.46 cm2)

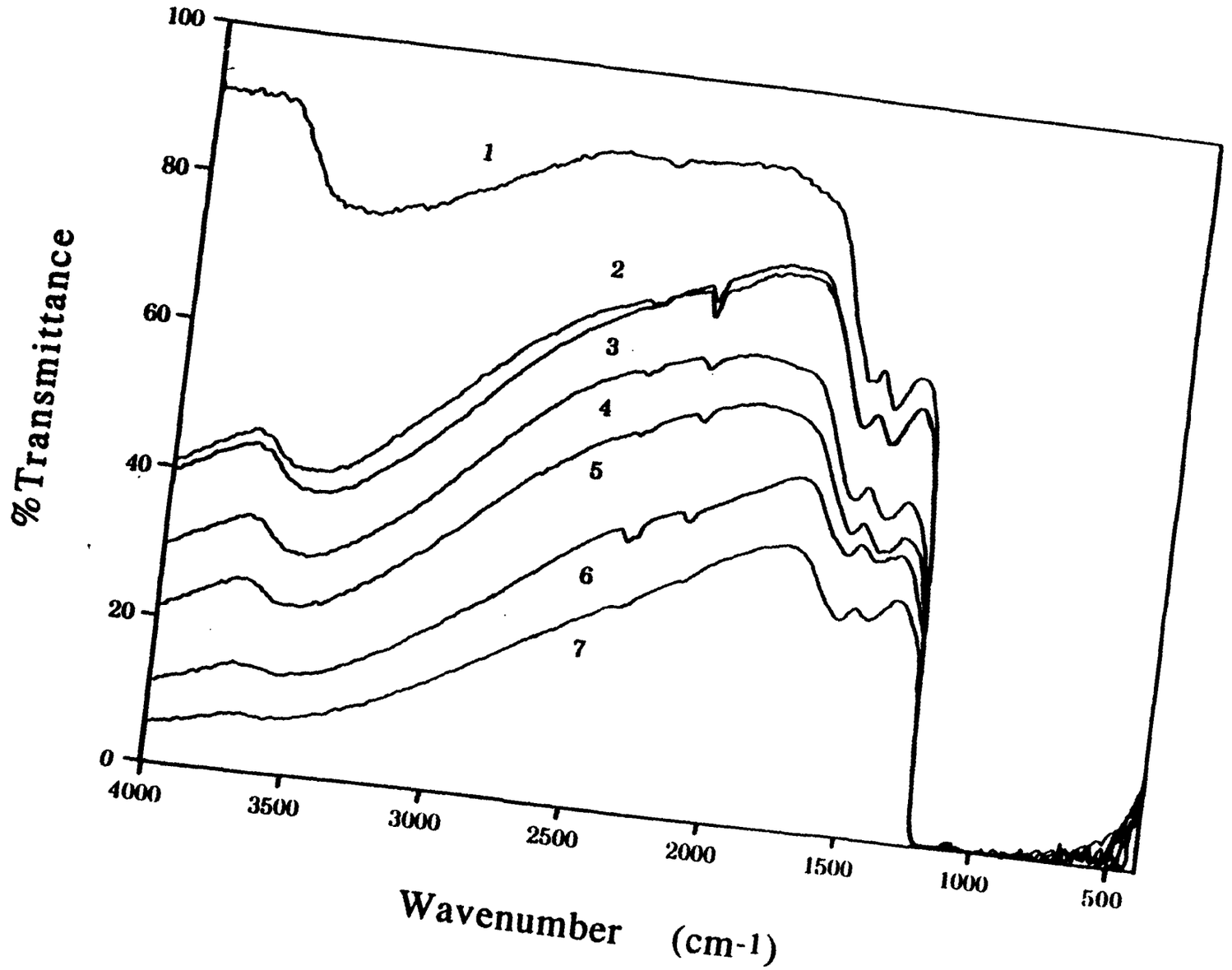
100
80
60
40
20
0
% Transmittance
1
2
3
4
5
6
7
4000
3500
3000
2500
2000
1500
1000
500
Wavenumber (cm-1)

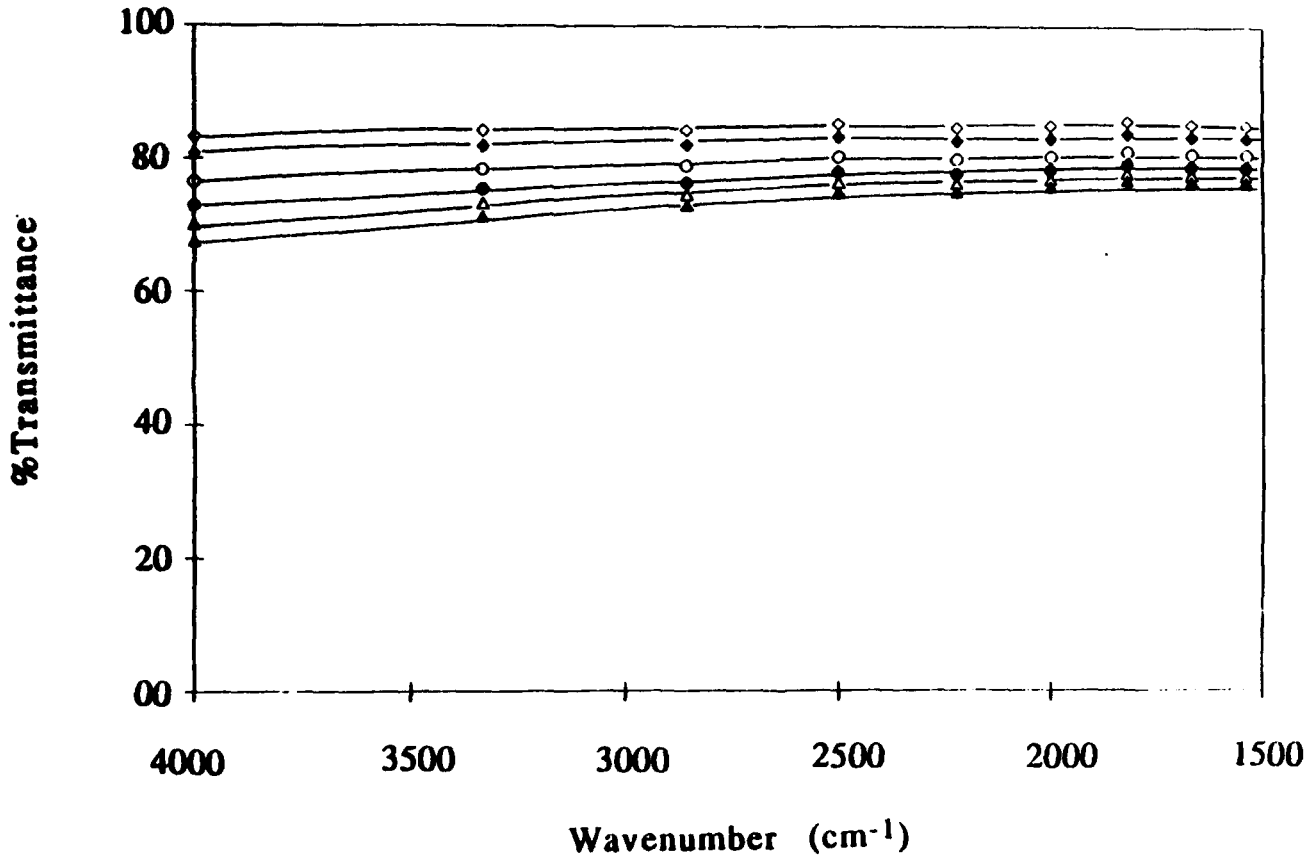
100
80
60
40
20
00
%Transmittance
4000
3500
3000
2500
2000
1500
Wavenumber (cm-1)

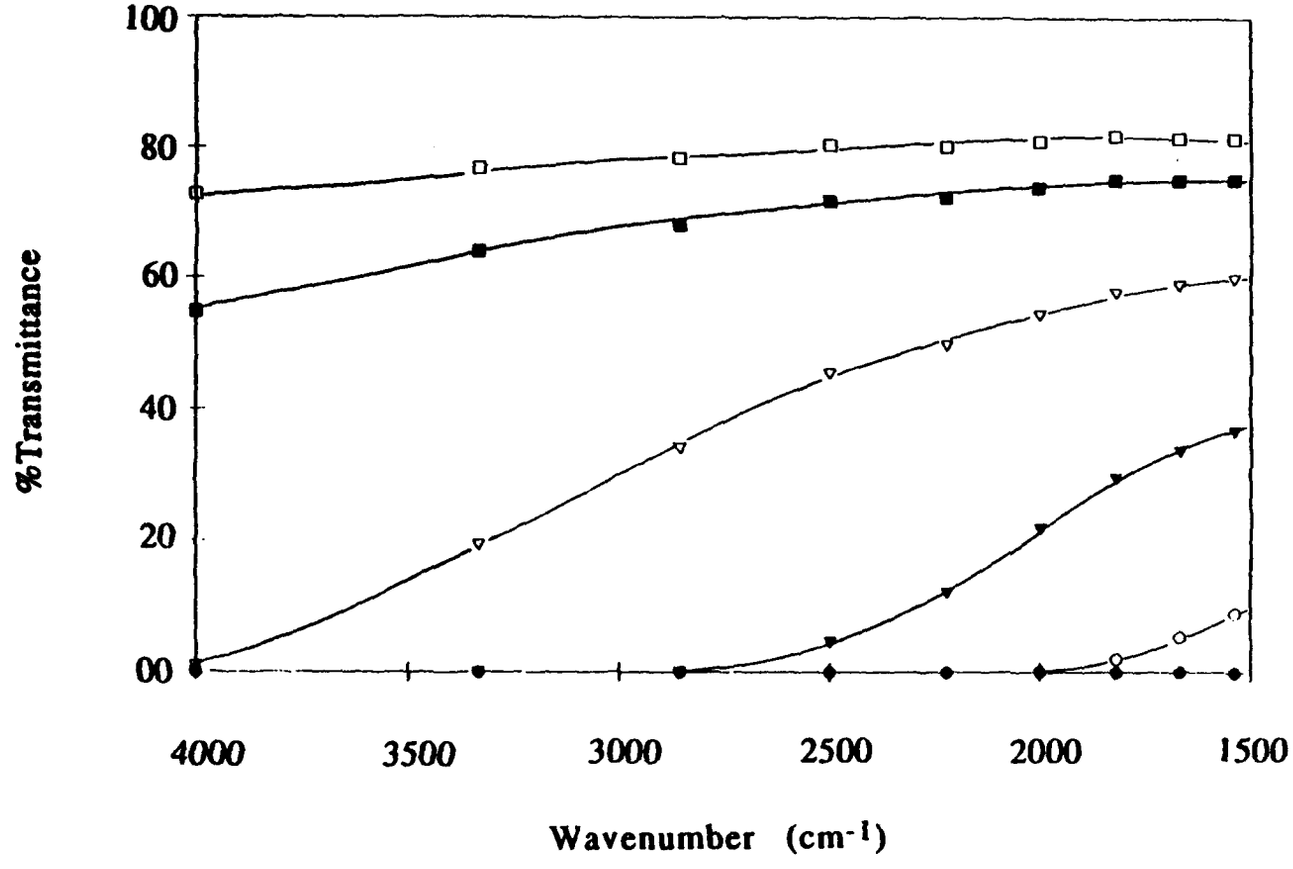
100
80
60
40
20
00
%Transmittance
4000
3500
3000
2500
2000
1500
Wavenumber (cm-1)

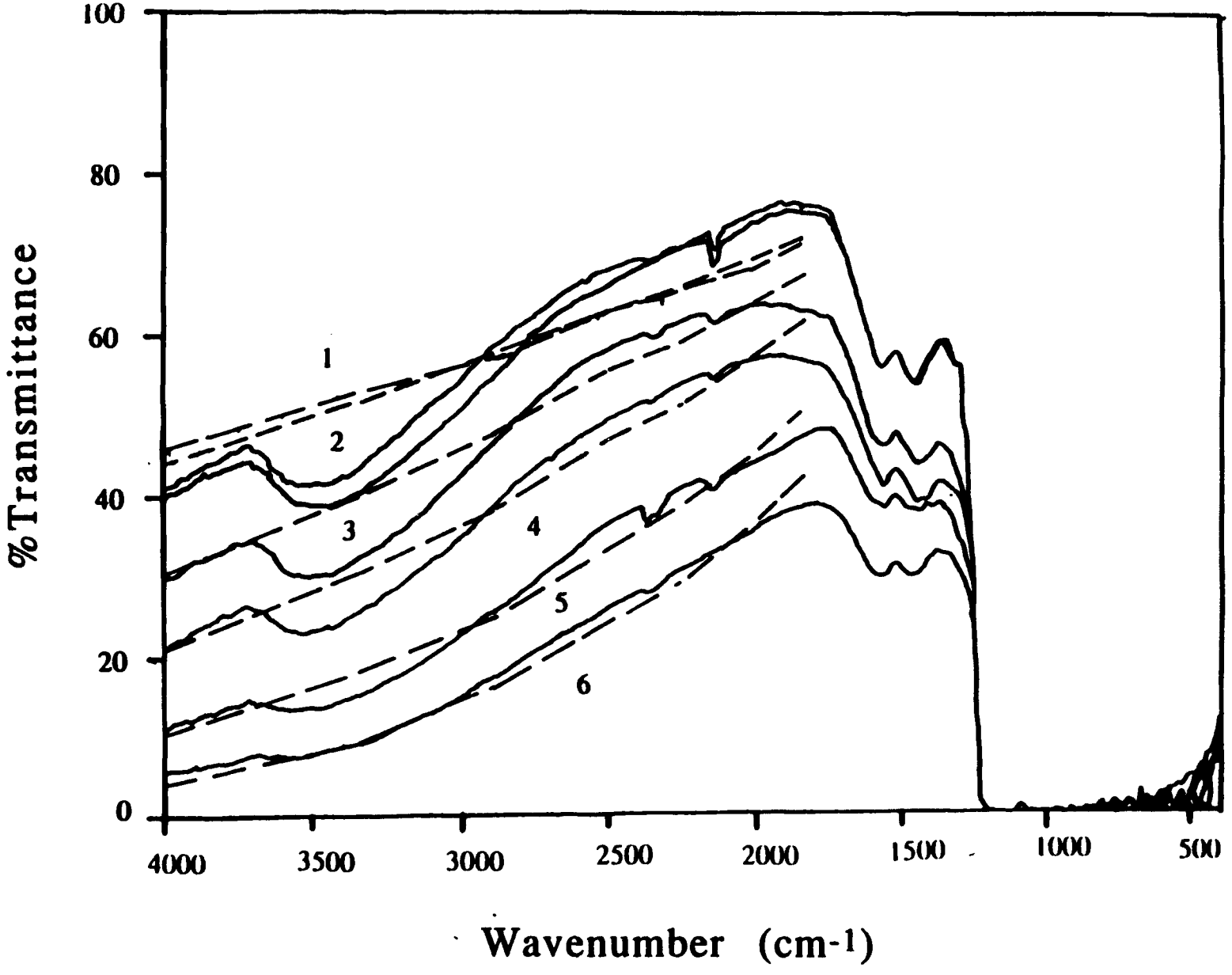
100
80
60
40
20
0
% Transmittance
1
2
3
4
5
6
4000
3500
3000
2500
2000
1500
1000
500
Wavenumber (cm-1)